

# **SURVEYING DIFFERENT MAGNETOCALORIC MATERIALS USING AN ACTIVE MAGNETIC REGENERATIVE REFRIGERATOR (AMRR) FOR HYDROGEN LIQUEFACTION**

**Mohamed G. Gado\*, Tsuyoshi Shirai, Kyohei Natsume, Akira Uchida,  
Takenori Numazawa, Koji Kamiya**

National Institute for Materials Science  
Tsukuba, 305-0003, Japan, mohamed.gado@nims.go.jp

## **ABSTRACT**

Hydrogen serves as a key clean energy carrier for decarbonization. Liquefied hydrogen offers high volumetric energy density for efficient storage and transport. However, its low liquefaction temperature of 20 K makes the process energy-intensive. This study investigates magnetic refrigeration as a potential method to enhance hydrogen liquefaction efficiency. Utilizing the magnetocaloric effect (MCE), magnetic refrigeration enables an efficient cooling cycle, which reduces energy consumption in the liquefaction process. Herein, granular  $\text{HoAl}_2$  particles have been proposed, given their significant specific heat and strong MCE. To boost the temperature span, an Active Magnetic Regenerative Refrigerator (AMRR) is deployed. In the present study, different magnetocaloric materials have been utilized to examine the hydrogen liquefaction efficiency in comparison to  $\text{HoAl}_2$ . The cooling power and coefficient of performance are systematically evaluated using heat transfer, fluid flow, and magnetic field cycling of the numerical AMRR model. Accordingly, the hydrogen liquefaction efficiency ( $\eta_{II}$ ) and hydrogen yield are evaluated, under an applied magnetic field of 5 T to quantify their impact on system-level performance. The results show a potential second-law efficiency ( $\eta_{II}$ ) over 60% and cooling capacity over 100 W using  $\text{HoAl}_2$  under an operating range of 20–30 K. On the other hand,  $\text{ErAl}_2$  can achieve a  $\eta_{II}$  over 40% and cooling capacity over 40 W under the operating range of 10–20 K. Taking advantage of those materials will eventually upgrade hydrogen utilization and push boundaries toward achieving a hydrogen society.

**Keywords:** Magnetic refrigeration, Hydrogen liquefaction, strong MCE

## **1. INTRODUCTION**

Green hydrogen, generated through electrolyzers powered by renewable energy sources, represents a critical instrument for climate change mitigation by enabling the decarbonization of energy-intensive sectors. In particular, traditional coal-based steel production is responsible for about 7% of global carbon dioxide emissions, and hydrogen presents a more sustainable and lower-carbon alternative (Gado, 2026). Hydrogen is decreasing reliance on conventional fossil fuels through the facilitation of domestically produced renewable hydrogen (Kavousighahfarokhi et al., 2026). It also plays a central role in Power-to-X pathways, fostering sectoral integration across the electricity, transportation, and industrial domains. Besides the hydrogen industrial relevance, it can effectively work as an energy storage carrier, which can contribute to grid stability and efficient energy management in buildings (Li and Deussen, 2025; Mastoi et al., 2025). Compared to the hydrogen gaseous form, liquid hydrogen exhibits substantially greater volumetric energy density, as liquefaction reduces its volume by nearly three orders of magnitude, making it effectively suitable for storage and transport (Gado et al., 2025). Nevertheless, hydrogen liquefaction is energy-intensive due to

its low liquefaction temperature of 20 K (Matsumoto et al., 2011). Therefore, boosting the efficiency of hydrogen liquefaction is crucial for advancing the technological and commercial development of the hydrogen value chain.

After hydrogen liquefaction by Sir James Dewar in 1898, multiple liquefaction systems have been developed. Conventional methods encompass Joule–Thomson and turbine expansion systems (e.g., the Linde–Hampson, Claude, Brayton, Collins, and mixed refrigerant cycles). Adversely, they are energy-intensive, requiring about 10–20 kWh/kg (Zhang et al., 2023), and achieve overall liquefaction efficiencies of only about 20–30% (Matsumoto et al., 2009). By contrast, magnetic refrigeration has recently emerged as a promising substitute for conventional liquefaction systems. This solid-state cooling technology operates based on the magnetocaloric effect (MCE), whereby the temperature of a magnetic material changes in response to variations in the magnetic field. (Gschneidner and Pecharsky, 2008; Pecharsky and Gschneidner Jr, 1999). Magnetic refrigeration systems are considered efficient, compact, and environmentally friendly, as they do not rely on ozone-depleting or greenhouse gases such as chlorofluorocarbons (CFCs) and hydrofluorocarbons (HFCs).

Figure 1 shows the classifications of magnetic refrigeration systems, namely adiabatic demagnetization refrigeration (ADR), Carnot magnetic refrigeration (CMR), and active magnetic regenerative refrigeration (AMRR). The ADR systems were successfully used to attain an ultra-low temperature of 0.25 K (Giauque and MacDougall, 1935). ADR systems operate based on the Carnot cycle and are widely applied in advanced technologies, including quantum computing and space instrumentation (Shirron, 2014). Similarly, CMR systems, which are also based on the Carnot cycle, have been explored for hydrogen liquefaction. Several studies have investigated the feasibility of CMR systems. For example, Ohira et al. liquified hydrogen using a pulsed magnet, reaching a second-law efficiency ( $\eta_{II}$ ) of 37% with a cooling capacity of 0.4 W (Ohira et al., 2000). In addition, Kamiya et al. (Kamiya et al., 2007) developed a hydrogen liquefaction system using a reciprocating CMR system operating under a stationary magnetic field.

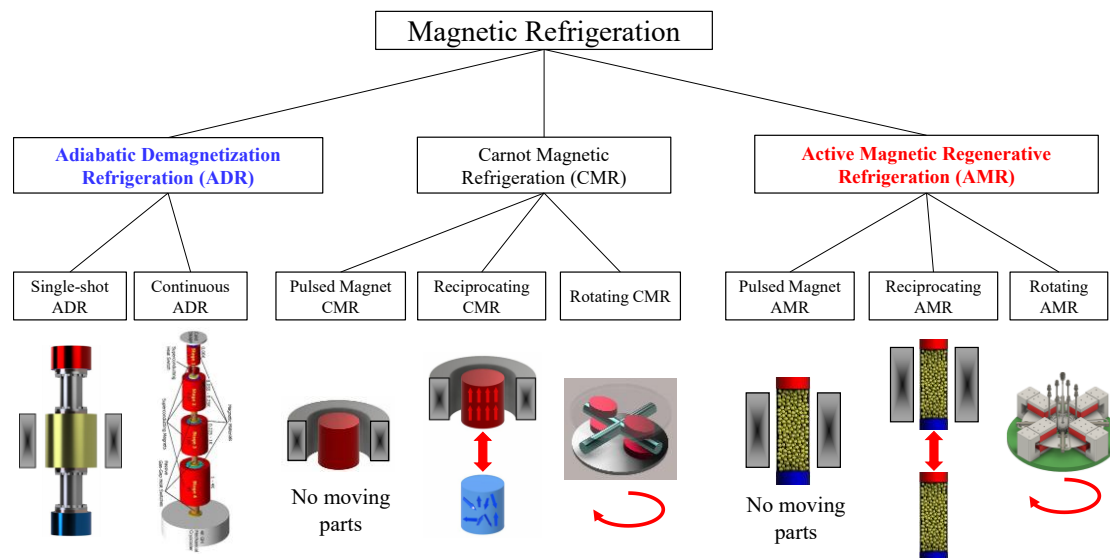


**Figure 1: Classification of magnetic refrigeration systems.**

Regarding the latest developments in producing liquid hydrogen using AMRR, Jeong et al. (Jeong et al., 1994) developed an AMRR system operating between 4.2 and 1.8 K, achieving continuous cooling to 1.8 K by alternately driving reciprocating flow through two regenerators with a superconducting coil. More recently, Kamiya et al. (Kamiya et al., 2025) assessed a hydrogen liquefier magnetized by a superconducting magnet, reporting a cooling capacity of 7.34 W with a  $\eta_{II}$  of 60.5%.

The importance of the present study is to highlight new magnetocaloric material candidates for hydrogen liquefaction. The deployment of  $\text{HoAl}_2$  indicated a significant hydrogen production yield. Meanwhile,  $\text{ErAl}_2$  showed an appreciable potential to provide further lower cryogenic temperatures than  $\text{HoAl}_2$ .

## 2. WORKING PRINCIPLES OF THE AMRR CYCLE FOR HYDROGEN LIQUEFACTION

In magnetic refrigeration systems, as illustrated in Fig. 2, subjecting a magnetic field to a magnetic refrigerant causes it to release heat, while removing the magnetic field allows it to absorb heat. The magnetization process is analogous to compression in conventional gas refrigeration, and demagnetization is comparable to expansion. In gas-based systems, cooling performance mainly depends on the gas compression ratio. Similarly, in magnetic refrigeration, the entropy change induced by magnetization serves a comparable function to the compression ratio in determining refrigeration capacity.

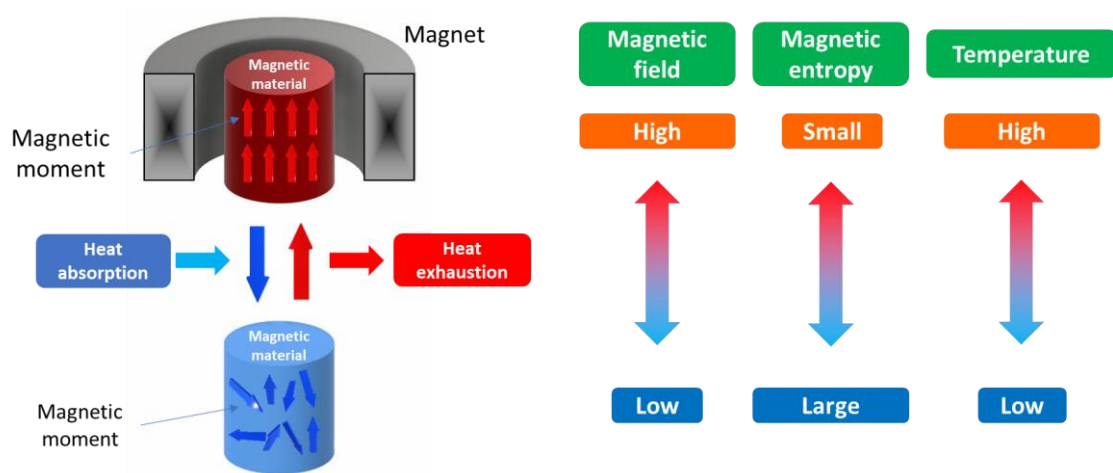


Figure 2: Schematic diagram of the AMRR cycle.

The AMRR cycle includes four stages, namely, (i) magnetization, (ii) cold-to-hot blow, (iii) demagnetization, and (iv) hot-to-cold blow (cf. Fig. 3). During the cold-to-hot end blow, the helium flow is allowed to reject heat to the hot-end heat exchanger (HHEX). During the hot-to-cold blow, helium gas is used to cover a cooling load via the cold-end heat exchanger (CHEX). Consecutive cycle operations enable a quasi-continuous cooling effect, which can be used for hydrogen liquefaction.

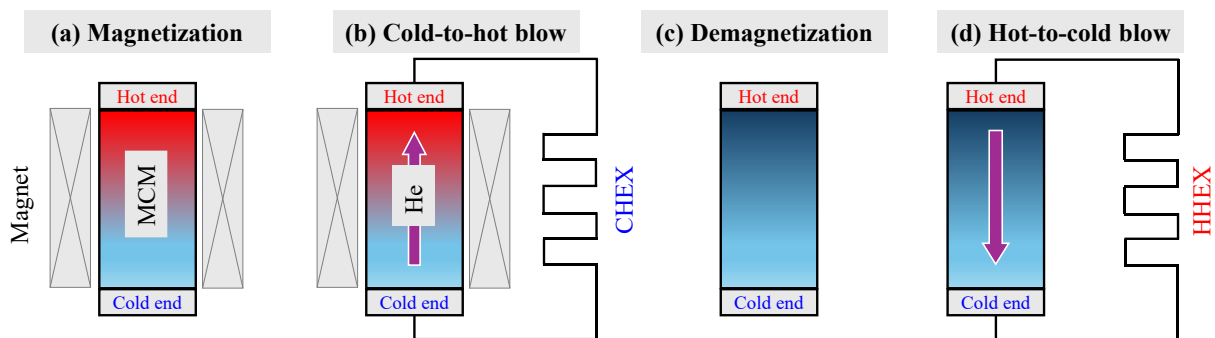


Figure 3: Schematic diagram of the AMRR cycle.

Extensive research has been carried out on different candidates of magnetocaloric materials for hydrogen liquefaction. Amongst them,  $\text{HoAl}_2$  and  $\text{ErAl}_2$  possess a strong magnetocaloric effect near the liquefaction temperature of hydrogen (20.3 K) (Gado et al., 2026). Each candidate has its local operating temperature range between the heat rejection and absorption reservoirs. In Fig. 4,  $\text{HoAl}_2$  shows a strong MCE near the

hot-end temperature of 30 K. Besides, it has a wide distribution of MCE, making it more suitable for hydrogen liquefaction applications. Mainly, at a magnetic field change of 5 T, both  $\text{ErAl}_2$  and  $\text{HoAl}_2$  show significant isothermal entropy changes that vary with temperature. For  $\text{ErAl}_2$ ,  $\Delta S$  increases rapidly with temperature, reaching a maximum of about 33 J/kg·K near 10–12 K, and then gradually decreases at higher temperatures. In contrast,  $\text{HoAl}_2$  exhibits its peak  $\Delta S$  of around 28–29 J/kg·K at a higher temperature of about 28–30 K, after which it steadily declines. This behavior reflects how each material responds to the applied magnetic field, with the largest entropy changes occurring near their respective magnetic transition temperatures. However,  $\text{HoAl}_2$  can be more expensive than  $\text{ErAl}_2$ .

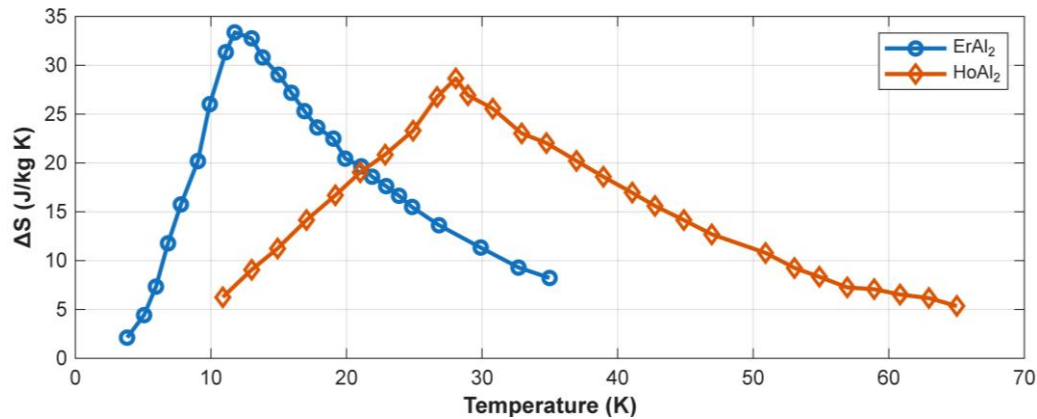


Figure 4: Isothermal entropy changes for  $\text{HoAl}_2$  and  $\text{ErAl}_2$ .

### 3. COMPUTATIONAL ANALYSIS

#### 3.1. NbTi superconducting magnet design

Magnetizing the MCM is produced using a NbTi superconducting magnet, two sets of coils (cf. Fig. 5a). The main coils provide the magnetic field of the magnet set, while the shield coils are used to curtail the effect of the magnet field and the top and bottom, enabling reduced stroke movement. Fig. 5b shows the magnetic field contours, which demonstrate the capability of generating a magnetic field over 5 T.

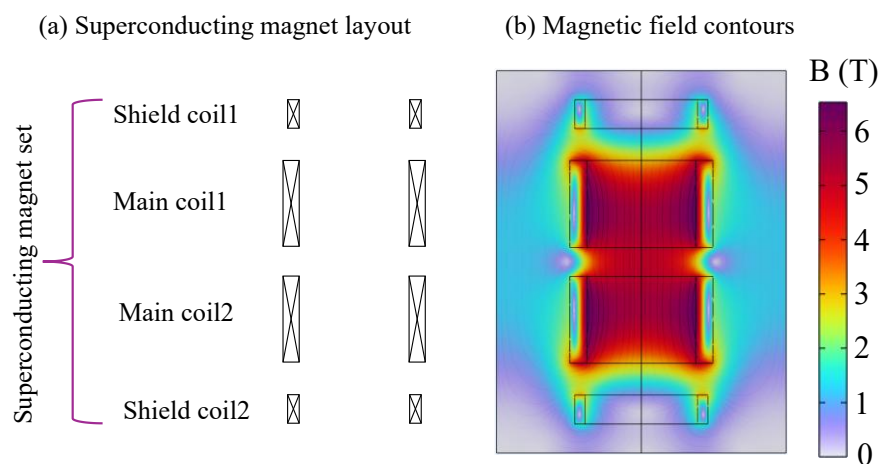
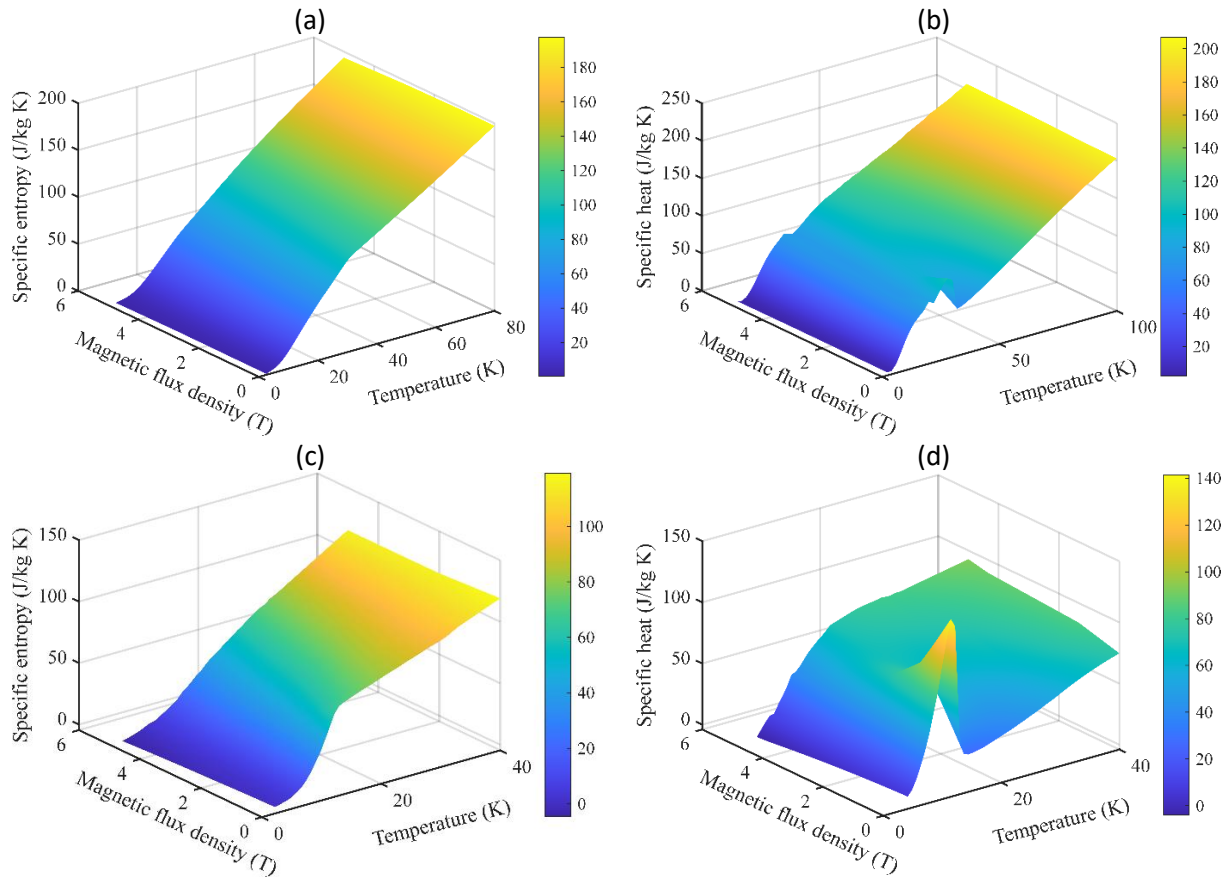


Figure 5: (a) Superconducting magnet layout, and (b) magnetic field contours.

### 3.2. Magnetocaloric materials

The main characteristics of HoAl<sub>2</sub> and ErAl<sub>2</sub> are shown in Fig. 6, including the specific entropy and heat capacity. Meanwhile, Table 1 lists their respective density and thermal conductivity.



**Figure 6. (a) specific entropy of HoAl<sub>2</sub>, (b) specific heat of HoAl<sub>2</sub>, (c) specific entropy of ErAl<sub>2</sub>, and (d) specific heat of ErAl<sub>2</sub>, at different magnetic densities (Hashimoto et al., 1986).**

**Table 2 Physical properties of HoAl<sub>2</sub> and ErAl<sub>2</sub> (Lopatina et al., 2022; Yamamoto et al., 2022).**

Property	HoAl <sub>2</sub>	ErAl <sub>2</sub>
Density (kg/m <sup>3</sup> )	6220	6250
Thermal conductivity (W/m K)	2	1

### 3.3. AMRR thermos-fluid coupling

#### 3.3.1. Continuity equation (compressed flow)

$$\frac{\partial(\rho_f)}{\partial t} + \nabla \cdot (\rho_f u) = 0 \quad \text{Eq. (1)}$$

#### 3.3.2. Momentum equation

$$\frac{1}{\varepsilon_b} \frac{\partial(\rho_f u)}{\partial t} + \frac{1}{\varepsilon_b^2} \rho_f u \cdot \nabla u = -\nabla p + \frac{\mu_f}{\varepsilon_b} \nabla^2 u - \frac{\mu_f}{\kappa} u \quad \text{Eq. (2)}$$

here,  $\varepsilon_b$  and  $\mu_f$  stand for the porosity of the AMRR bed and HTF dynamic viscosity, respectively.

### 3.3.3. Energy equation

$$(1 - \varepsilon_b) \rho_s C_{p,s} \frac{\partial T_s}{\partial t} = \nabla \cdot [(1 - \varepsilon) k_s \nabla T_s] + A_s h_{sf} (T_f - T_s) + (1 - \varepsilon_b) Q_S \quad \text{Eq. (3)}$$

$$\rho_f C_{p,f} \left( \frac{\partial T_f}{\partial t} + \mathbf{u} \cdot \nabla T_f \right) = k_f \nabla^2 T_f + \frac{A_s h_{sf}}{\varepsilon_b} (T_s - T_f) \quad \text{Eq. (4)}$$

here,  $T_s$  refers to the MCM temperature, and  $T_f$  stands for the HTF temperature. The MCM density, specific heat, and thermal conductivity are assigned as  $\rho_s$ ,  $C_{p,s}$ , and  $k_s$ .

### 3.3.4. The magnetocaloric source term

$$Q_S = - \rho_s T_s \frac{\partial S}{\partial B} \dot{B} \quad \text{Eq. (5)}$$

where  $\dot{B}$  is the magnetic field ramp rate. Eventually, Table 3 categorized the main characteristics of the AMRR system.

**Table 3 Main characteristics of the AMRR system.**

AMRR characteristics	HoAl <sub>2</sub>	ErAl <sub>2</sub>
$T_H$	30 (K)	20 (K)
$T_C$	20 (K)	10 (K)
$\varepsilon_b$	0.392 (–)	0.392 (–)
$d_p$	300 (μm)	300 (μm)

### 3.3.5. Performance indicators

In this section, different performance indicators are evaluated, namely (Zheng et al., 2024):

Cooling power:

$$Q_C = \frac{1}{t_{cycle}} \int_0^{t_{cycle}} \dot{m}_f C_{p,f} (T_C - T_{C,out}) dt \quad \text{Eq. (6)}$$

Rejected heat (Zheng et al., 2024):

$$Q_H = \frac{1}{t_{cycle}} \int_0^{t_{cycle}} \dot{m}_f C_{p,f} (T_{H,out} - T_H) dt \quad \text{Eq. (7)}$$

Coefficient of performance:

$$COP = \frac{Q_C}{Q_H - Q_C} \quad \text{Eq. (8)}$$

Second-law efficiency ( $\eta_{II}$ ):

$$\eta_{II} = \frac{COP}{COP_{Carnot}} \times 100\% \quad \text{Eq. (9)}$$

Hydrogen liquefaction rate:

$$\dot{m}_{H_2} = \frac{Q_C}{\Delta h_{total}} \quad \text{Eq. (10)}$$



The total enthalpy difference:

$$\Delta h_{\text{total}} = (h_{80\text{K},0.25\text{MPa}} - h_{x=1,0.25\text{MPa}}) + (h_{x=1,0.25\text{MPa}} - h_{x=0,0.25\text{MPa}}) \quad \text{Eq. (11)}$$

herein,  $x$  denotes the vapor quality. Besides, hydrogen gas is presumably kept initially at 30 K and 0.25 MPa.

#### 4. RESULTS AND DISCUSSION

The following section presents the potential application of HoAl<sub>2</sub> and ErAl<sub>2</sub>. For HoAl<sub>2</sub>, it is examined with the best operating range of 20-30 K, whereas ErAl<sub>2</sub> is examined with 10-20 K. Also, the impact of the helium mass flow rate is sensitively investigated with 80-160 g/s. Figure 7 illustrates the transient behavior of a magnetic refrigeration system over one complete operating cycle of approximately 14.6 seconds, showing temperature evolution at the hot and cold ends (top row) and the corresponding cooling power (bottom row) for two different operating conditions. The cycle is divided into four stages: magnetization (Mag), cold-to-hot heat transfer (C→H), demagnetization (Demag), and hot-to-cold heat transfer (H→C). During magnetization, the hot-end temperature rises due to the MCE, while the cold-end exhibits a smaller temperature rise (because of the lower effect of the magnetic flux). During demagnetization, the hot-end temperature decreases, and the cold end cools further (due to the significant effect of magnetic flux reduction). In Fig. 7b, for ErAl<sub>2</sub>, a sharper temperature drop at the cold end and a larger temperature span compared to HoAl<sub>2</sub> are shown, which indicates the stronger MCE at the cold end (at 20 K) for ErAl<sub>2</sub>. Figs. 7c and d show the cooling power evolution for HoAl<sub>2</sub> and ErAl<sub>2</sub>, respectively. It can be seen that HoAl<sub>2</sub> shows a higher cooling power peak than ErAl<sub>2</sub>.

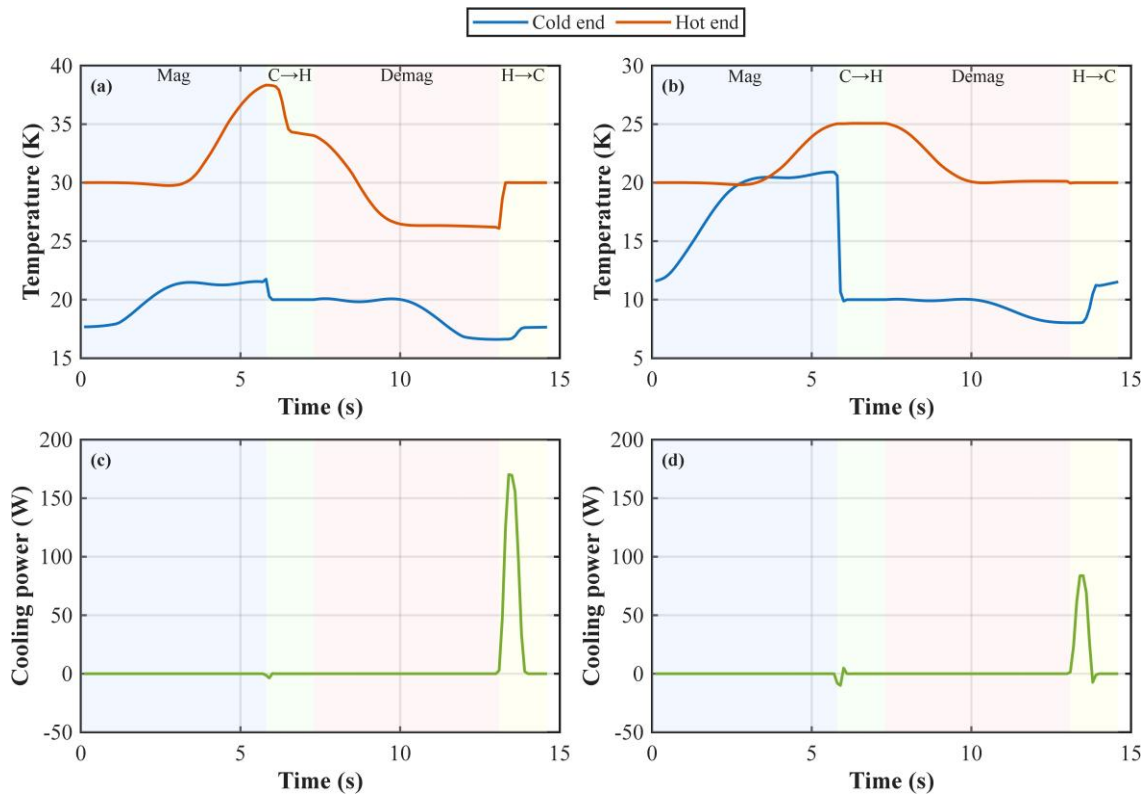
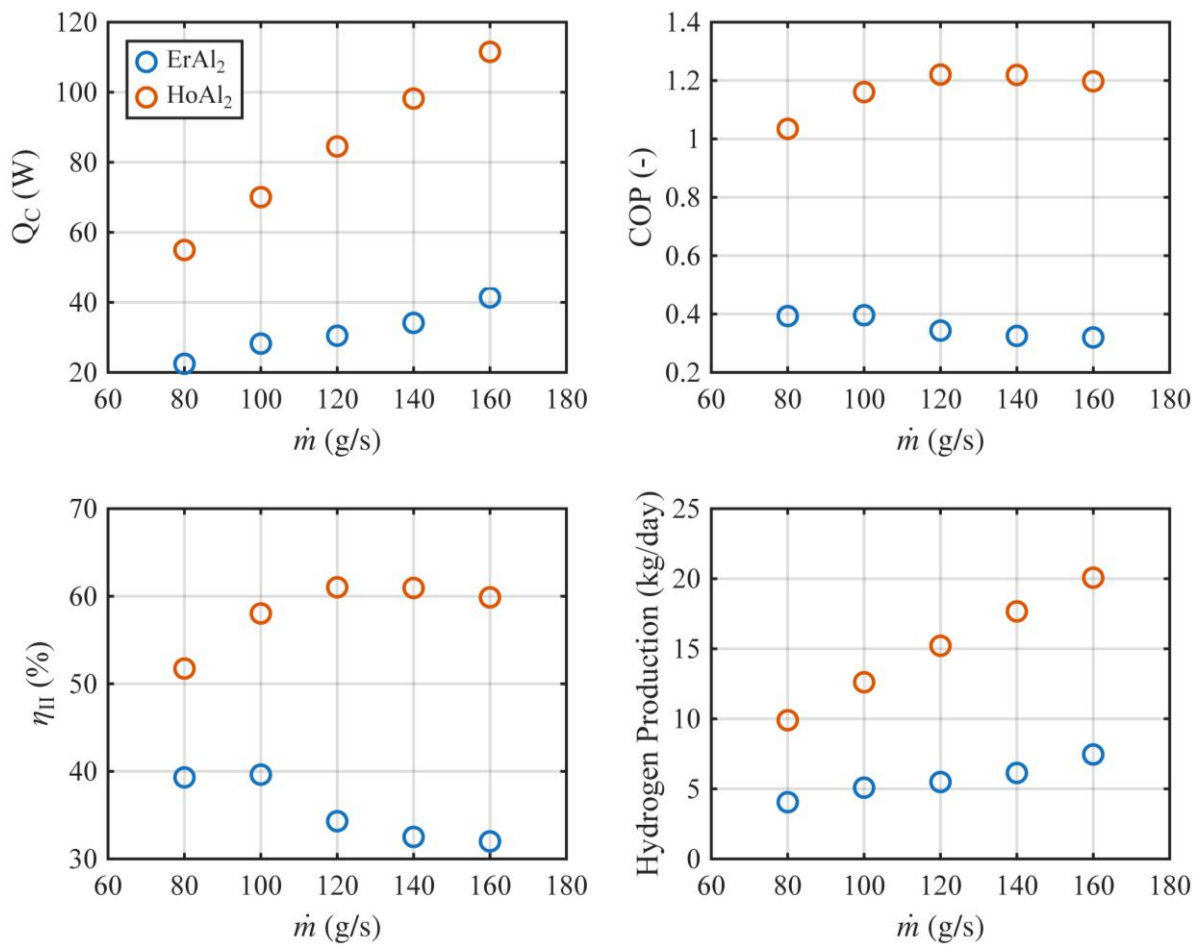


Figure 7. Cycle evolution of AMRR temperature and cooling capacity for HoAl<sub>2</sub> and ErAl<sub>2</sub>.

Figure 8 compares the performance of  $\text{ErAl}_2$  and  $\text{HoAl}_2$  magnetic refrigerants with the variation in helium mass flow rate ( $\dot{m} = 80\text{--}160$  g/s), evaluating  $Q_c$ , COP,  $\eta_{II}$ , and hydrogen yield. The  $Q_c$  increases steadily with mass flow rate for both materials; however,  $\text{HoAl}_2$  consistently delivers significantly higher cooling power.  $\text{ErAl}_2$  rises from approximately 22 W to 41 W, while  $\text{HoAl}_2$  increases from about 55 W to 112 W, indicating nearly 2.5–3 times greater cooling capacity across the range. The COP behavior differs between the two materials. For  $\text{ErAl}_2$ , COP decreases gradually from about 0.39 to 0.32 as mass flow rate increases, showing reduced thermodynamic efficiency at higher flow rates. By contrast,  $\text{HoAl}_2$  exhibits much higher efficiency, with a COP of over 1.22 near 120–140 g/s.

Similarly, the  $\eta_{II}$  decreases from roughly 39% to 32% with increasing flow rate  $\text{ErAl}_2$ . Whereas  $\text{HoAl}_2$  increases from 52% to about 61% at 120–140 g/s and then marginally declines. Accordingly,  $\text{HoAl}_2$  demonstrates superior performance due to the proximity of its transition temperature (about 27 K) to the heat rejection temperature of 30 K. Meanwhile, hydrogen daily yield increases nearly linearly with mass flow rate for both materials.  $\text{ErAl}_2$  rises from approximately 4.0 to 7.45 kg/day, while  $\text{HoAl}_2$  increases from about 9.9 to 20.1 kg/day, almost doubling the hydrogen output compared to  $\text{ErAl}_2$ . Overall,  $\text{HoAl}_2$  outperforms  $\text{ErAl}_2$  in cooling capacity, efficiency,  $\eta_{II}$ , and hydrogen production across all tested mass flow rates.



**Figure 8. Impact of the He mass flow rate on the AMRR cooling power, COP,  $\eta_{II}$ , and hydrogen yield, for  $\text{HoAl}_2$  and  $\text{ErAl}_2$ .**



## 5. CONCLUSIONS

A quantitative comparison was developed using  $\text{HoAl}_2$  and  $\text{ErAl}_2$  to examine the potential for efficient hydrogen liquefaction. Based on the aforementioned findings, the following concluding points can be inferred:

- $\text{HoAl}_2$  can optimally work within the operating range of 20-30 K and flow rate range of 80-160 g/s, highlighting a cooling throughput of 112 W, a coefficient of performance of 1.2, and  $\eta_{II}$  of 61%.
- $\text{ErAl}_2$  has a significant magnetic effect at temperatures below 20 K, operating down to 13 K, below the hydrogen triple point.

## ACKNOWLEDGEMENTS

This work was supported by the JST-Mirai Program Grant Number JPMJMI18A3, Japan. We also acknowledge the financial support provided by the Japan Society for the Promotion of Science (JSPS).

## NOMENCLATURE

$A_s$	Specific surface area of particles ( $\text{m}^2 \cdot \text{m}^{-3}$ )	$S$	Entropy ( $\text{J} \cdot \text{kg}^{-1} \cdot \text{K}^{-1}$ )
$B$	Magnetic flux density (T)	$t$	Time (s)
$C_{p,f}$	Specific heat capacity of fluid ( $\text{J} \cdot \text{kg}^{-1} \cdot \text{K}^{-1}$ )	$t_{cycle}$	AMRR cycle time (s)
$C_{p,s}$	Specific heat capacity of solid ( $\text{J} \cdot \text{kg}^{-1} \cdot \text{K}^{-1}$ )	$T$	Temperature (K)
$d_p$	Particle diameter (mm)	$T_f$	Fluid temperature (K)
$h_{sf}$	Solid–fluid heat transfer coefficient ( $\text{W} \cdot \text{m}^{-2} \cdot \text{K}^{-1}$ )	$T_s$	Solid temperature (K)
$h$	Specific enthalpy ( $\text{J} \cdot \text{kg}^{-1}$ )	$T_H$	Hot-end temperature (K)
$k_f$	Thermal conductivity of fluid ( $\text{W} \cdot \text{m}^{-1} \cdot \text{K}^{-1}$ )	$T_C$	Cold-end temperature (K)
$k_s$	Thermal conductivity of solid ( $\text{W} \cdot \text{m}^{-1} \cdot \text{K}^{-1}$ )	$T_{H,out}$	Fluid outlet temperature at hot end (K)
$\dot{m}_f$	Mass flow rate of fluid ( $\text{kg} \cdot \text{s}^{-1}$ )	$T_{C,out}$	Fluid outlet temperature at cold end (K)
$\dot{m}_{H_2}$	Hydrogen liquefaction rate ( $\text{kg} \cdot \text{s}^{-1}$ )	$u$	Superficial fluid velocity vector ( $\text{m} \cdot \text{s}^{-1}$ )
$Q_C$	Cooling power (W)	$V$	Molar volume ( $\text{m}^3 \cdot \text{mol}^{-1}$ )
$Q_H$	Rejected heat (W)	$x$	Vapor quality (–)
$Q_S$	Magnetocaloric heat source ( $\text{W} \cdot \text{m}^{-3}$ )	$\Delta h_{total}$	Total enthalpy difference ( $\text{J} \cdot \text{kg}^{-1}$ )
$R$	Universal gas constant ( $\text{J} \cdot \text{mol}^{-1} \cdot \text{K}^{-1}$ )		

## REFERENCES

- Gado, M.G., 2026. Green hydrogen: A key energy carrier replacing fossil fuels across multiple sectors. *Renew. Sustain. Energy Rev.* 230, 116683. <https://doi.org/https://doi.org/10.1016/j.rser.2025.116683>
- Gado, M.G., Al-Ghussain, L., Alrbai, M., Al-dahidi, S., 2025. Sustainable e-fuels production , liquefaction and transport technoeconomic feasibility using renewable energy resources. *Energy Convers. Manag.* 345, 120373. <https://doi.org/10.1016/j.enconman.2025.120373>
- Gado, M.G., Shirai, T., Yoshida, Y., Uchida, A., Hirayama, T., Numazawa, T., Natsume, K., Kamiya, K., 2026. Experimental assessment and comparative analysis of active magnetic regenerative refrigeration for hydrogen liquefaction using  $\text{HoAl}_2$  and  $\text{ErAl}_2$ . *Cryogenics (Guildf)*. 158, 104347. <https://doi.org/https://doi.org/10.1016/j.cryogenics.2026.104347>
- Giauque, W.F., MacDougall, D.P., 1935. The Production of Temperatures below One Degree Absolute by Adiabatic Demagnetization of Gadolinium Sulfate. *J. Am. Chem. Soc.* 57, 1175–1185.

<https://doi.org/10.1021/ja01310a007>

- Gschneidner, K.A., Pecharsky, V.K., 2008. Thirty years of near room temperature magnetic cooling: Where we are today and future prospects. *Int. J. Refrig.* 31, 945–961. <https://doi.org/https://doi.org/10.1016/j.ijrefrig.2008.01.004>
- Hashimoto, T., Matsumoto, K., Kurihara, T., Numazawa, T., Tomokiyo, A., Yayama, H., Goto, T., Todo, S., Sahashi, M., 1986. Investigations on the Possibility of the RAl<sub>2</sub> System as a Refrigerant in an Ericsson Type Magnetic Refrigerator BT - Advances in Cryogenic Engineering Materials, in: Reed, R.P., Clark, A.F. (Eds.), . Springer US, Boston, MA, pp. 279–286. [https://doi.org/10.1007/978-1-4613-9871-4\\_33](https://doi.org/10.1007/978-1-4613-9871-4_33)
- Jeong, S., Smith, J.L., Iwasa, Y., 1994. Tandem magnetic refrigerator for 1.8 K. *Cryogenics (Guildf)*. 34, 263–269. [https://doi.org/https://doi.org/10.1016/0011-2275\(94\)90105-8](https://doi.org/https://doi.org/10.1016/0011-2275(94)90105-8)
- Kamiya, K., Natsume, K., Uchida, A., Numazawa, T., Shirai, T., Saito, A.T., Matsumoto, K., Masuyama, S., 2025. Hydrogen liquefaction by active magnetic regenerative refrigeration. *Cryogenics (Guildf)*. 152, 104205. <https://doi.org/https://doi.org/10.1016/j.cryogenics.2025.104205>
- Kamiya, K., Takahashi, H., Numasawa, T., Nozawa, H., Yanagitani, T., 2007. Hydrogen liquefaction by magnetic refrigeration. *Proc. 14th Int. Cryocooler Conf.* 637–644.
- Kavousighahfarokhi, A., Hannan, M.A., Ker, P.J., Wong, R.T.K., Ong, H.C., Begum, R.A., Hossain, M.J., Jang, G., 2026. Techno-economic analysis of hydrogen integrated microgrid and hydrogen refueling systems application: A sustainable energy solution. *Renew. Sustain. Energy Rev.* 226, 116379. <https://doi.org/https://doi.org/10.1016/j.rser.2025.116379>
- Li, Z., Deussen, D., 2025. Role of energy storage technologies in enhancing grid stability and reducing fossil fuel dependency. *Int. J. Hydrogen Energy* 102, 1055–1074. <https://doi.org/https://doi.org/10.1016/j.ijhydene.2024.12.489>
- Lopatina, A., Watanabe, S., Futatsuka, K., Kumazawa, N., Hirano, Y., Matsunaga, K., Abe, S., Matsumoto, K., Saito, A.T., Takeya, H., Numazawa, T., 2022. Thermal and electrical conductivity of magnetic refrigerant RT<sub>2</sub> Laves compounds (R: Rare earth; T: Al, Ni) for magnetic refrigerator application. *Cryogenics (Guildf)*. 126. <https://doi.org/10.1016/j.cryogenics.2022.103519>
- Mastoi, M.S., Wang, D., Zhou, X., He, X., Hassan, M., Ali, A., Rehman, A., 2025. Study of energy storage technology approaches for mitigating wind power fluctuations to enhance smart grid resilience. *Renew. Sustain. Energy Rev.* 224, 116072. <https://doi.org/https://doi.org/10.1016/j.rser.2025.116072>
- Matsumoto, K., Kondo, T., Ikeda, M., Numazawa, T., 2011. Numerical analysis of active magnetic regenerators for hydrogen magnetic refrigeration between 20 and 77K. *Cryogenics (Guildf)*. 51, 353–357. <https://doi.org/https://doi.org/10.1016/j.cryogenics.2010.06.003>
- Matsumoto, K., Kondo, T., Yoshioka, S., Kamiya, K., Numazawa, T., 2009. Magnetic refrigerator for hydrogen liquefaction. *J. Phys. Conf. Ser.* 150. <https://doi.org/10.1088/1742-6596/150/1/012028>
- Ohira, K., Nakamichi, K., Furumoto, H., 2000. Experimental Study on Magnetic Refrigeration for the Liquefaction of Hydrogen BT - Advances in Cryogenic Engineering, in: Shu, Q.-S. (Ed.), . Springer US, Boston, MA, pp. 1747–1754. [https://doi.org/10.1007/978-1-4615-4215-5\\_101](https://doi.org/10.1007/978-1-4615-4215-5_101)
- Pecharsky, V.K., Gschneidner Jr, K.A., 1999. Magnetocaloric effect and magnetic refrigeration. *J. Magn. Magn. Mater.* 200, 44–56. [https://doi.org/https://doi.org/10.1016/S0304-8853\(99\)00397-2](https://doi.org/https://doi.org/10.1016/S0304-8853(99)00397-2)

- Shirron, P.J., 2014. Applications of the magnetocaloric effect in single-stage, multi-stage and continuous adiabatic demagnetization refrigerators. *Cryogenics (Guildf)*. 62, 130–139.  
<https://doi.org/https://doi.org/10.1016/j.cryogenics.2014.03.014>
- Yamamoto, T.D., Takeya, H., Saito, A.T., Terashima, K., Numazawa, T., Takano, Y., 2022. Magnetocaloric particles of the Laves phase compound HoAl<sub>2</sub> prepared by electrode induction melting gas atomization. *J. Magn. Magn. Mater.* 547, 168906.  
<https://doi.org/https://doi.org/10.1016/j.jmmm.2021.168906>
- Zhang, T., Uratani, J., Huang, Y., Xu, L., Griffiths, S., Ding, Y., 2023. Hydrogen liquefaction and storage: Recent progress and perspectives. *Renew. Sustain. Energy Rev.* 176, 113204.  
<https://doi.org/https://doi.org/10.1016/j.rser.2023.113204>
- Zheng, W., Shen, J., Li, Z., Huang, H., Hai, P., Liu, J., Chen, Z., Gao, X., Mo, Z., 2024. Numerical simulation of a multistage magnetic refrigeration system in the temperature range of liquid hydrogen. *Int. J. Hydrogen Energy* 51, 523–535. <https://doi.org/https://doi.org/10.1016/j.ijhydene.2023.07.192>